PNAS
www.pnas.org

Supplementary Information for

Ammonia emission control in China would mitigate haze pollution and nitrogen deposition, but worsen acid rain

Mingxu Liu, Xin Huang, Yu Song, Jie Tang, Junji Cao, Xiaoye Zhang, Qiang Zhang, Shuxiao Wang, Tingting Xu, Ling Kang, Xuhui Cai, Hongsheng Zhang, Fumo Yang, Huanbo Wang, Jian Zhen Yu, Alexis K.H. Lau, Lingyan He, Xiaofeng Huang, Lei Duan, Aijun Ding, Likun Xue, Jian Gao, Bin Liu, & Tong Zhu

Correspondence to: songyu@pku.edu.cn or tzhu@pku.edu.cn

This PDF file includes:

www.pnas.org/cgi/doi/10.1073/pnas.1814880116

Materials and Methods

NH_3 emission and its abatement in China. NH_3 emission level and its spatial-temporal variation play a key role in the investigation of NH_3 on the environment. In this study, we adopted a comprehensive NH_3 emission inventory covering agricultural activities, biomass burning, industry, transportation and other non-agricultural sectors, developed by our research group (PKU-NH_3) (1, 2). To evaluate its reliability, we compared it with other databases in terms of emission magnitude and monthly variation.

As illustrated in Fig. S1A, the national annual emission was estimated to be 10.2 Tg in 2015 by the PKU-NH_3 model, which was consistent with those of MEIC and Paulot et al. (3). The emission from Zhang et al. (4) was about 20% higher than our study. The major difference was originated from mineral nitrogen fertilizer application (5.0 Tg in Zhang et al. vs. 3.1 Tg in PKU-NH_3), as they followed our methods in the estimation of livestock waste emissions. Another study using the bi-directional CMAQ model estimated nitrogen fertilizer NH_3 emissions at 3.0 Tg in 2011 (5), quite similar with our inventory. The results from REAS (6), Streets et al. (7) and EDGAR (http://edgar.jrc.ec.europa.eu/overview.php?v=432) were 30−50% higher than our inventory. Specifically, Streets et al. (7) used identical emission factors (EFs) for urea and ammonium bicarbonate fertilizers over China without considering the environmental conditions (e.g., soil pH, temperature, and application methods, etc.). In REAS v2.1 inventory for 2000−2008, the agricultural emissions were extrapolated from REAS v1.1 for 2000 by comparing the activity data in the target year to those in 2000. They did not consider the year-to-year changes in meteorological conditions and amounts of different types of fertilizer applied. As we have pointed out, these could lead to overestimation of NH_3 emissions from mineral fertilizer application (2). Moreover, modeling studies using Streets et al.'s NH_3 inventory suggested their emissions should be reduced by at least 20% in order to better simulate particulate nitrate (8). We have also applied our NH_3 inventory in air quality simulations, which showed a good performance in simulating particulate nitrate and ammonium (9).

Paulot et al. (3) and Zhang et al. (4) optimized their monthly emission estimates with observations of wet deposition and satellite, respectively, and we evaluated the monthly variation of our NH_3 emissions against these two studies (Fig. S1B). All inventories showed a consistent seasonal pattern of monthly NH_3 emissions, with largest fractions (35−40%) in summer (June, July and August, JJA) and smallest (10−15%) in (December, January and February, DJF) due to agricultural timings and meteorological conditions. In general, our self-developed NH_3 emission inventory was reasonable by the comparison with other inventories and its application in model simulations.

In China, nitrogen fertilization and extensive livestock industry contribute more than 80% of total NH_3 emissions. In the following, we provided detailed evidences to demonstrate the feasibility of large emission reductions from these agricultural

activities in China. For synthetic fertilizer application, Chinese farmers always adopt surface application (surface broadcast) of fertilizers in the topdressing process, which substantially promotes NH_3 loss compared to deep placement (1, 10). It will be effective to engage Chinese farmer in adopting science-based management practices for reducing nitrogen loss without compromising crop yields (11). Based on the PKU-NH_3 model, we find that NH_3 emissions from fertilization could be reduced about 50% by improving fertilizer application methods. Moreover, Chinese farmers apply excess synthetic nitrogen fertilizers to boost crop yields, which results in a low efficiency of nitrogen fertilizer and consequently enhanced NH_3 volatilization (12). Chinese agricultural scientists have indicated that fertilizer use in China can be reduced by at least 20% by optimizing nitrogen fertilization techniques (12) and increasing farm sizes (13).

For livestock industry, NH_3 emission is released through the whole manure management chain in farms including animal excretion in outdoors or houses, manure storage, and manure field application. Recent studies have recognized that inadequate manure collection and storage are the major causes of huge livestock NH_3 emissions in China (14). There is poor containment of manure as it is generated and processed (in yards, livestock buildings, manure stores and composting plants), with much putting in the open air or being directed to ditches and watercourses (15). Consequently, as much as 78% of the N excreted by animals are lost to the environment, mainly through NH_3 emissions (16). So improving livestock manure management can substantially reduce NH_3 emissions in farms. Various feasible measures have been proposed to mitigate NH_3 emissions in the livestock manure management chain, such as reducing the surface area and exposure time of manure in the house, covered storage, low protein feeding, and deep injection of manure in arable land (17). Specifically, low protein feeding is regarded as a cost-effective option in NH_3 emission control. This option can yield additional benefit since China wishes to put more low-protein feed in animal farms in order to reduce soybean imports (18).

Here, we estimated the reduction in NH_3 emissions in China from these agricultural sectors using the following equation,

$$E_i = A_i \times EF_i \times (1-\eta_i) \quad (1)$$

in which E represents estimated NH_3 emissions; i represents different agricultural production phases, including fertilizer application, livestock manure in house, manure storage, and manure application in arable land; A is the agricultural activity data; EF is the emission factor belonging to specific activity; and η represents the abatement efficiency, which depends on agricultural activity and effectiveness of abatement options. In the PKU-NH_3 model, the baseline scenario corresponded to $\eta = 0$, while a emission-control scenario was developed by applying feasible abatement options for NH_3 emission reduction, that is, reducing corresponding EFs or activity levels (only for resolving over-fertilization) in the model estimate. The abatement options and

their reduction efficiencies were listed in Table S1. Many studies have provided the mitigation potentials of these abatement options based on meta-analysis assessment (17, 19). These measures could yield larger effectiveness in China due to the current poor agricultural management compared to developed countries (16) (Table S2).

Model simulations. To quantify the influences of China's potential NH_3 emission reduction on $PM_{2.5}$ pollution and precipitation acidification, we performed simulations using Weather Research and Forecasting community model coupled chemistry modules online, WRF-Chem Version 3.6.1. WRF-Chem has been widely evaluated through field observations or satellite retrievals and it is applied as a powerful tool in researches of air pollution, aerosol-cloud-radiation interaction etc. (20-22). In this study, the baseline simulations were performed during JJA and DJF of 2015. Meanwhile, an emission-control scenario targeted for 2015−2020, with a 50% reduction in NH_3 emission and 15% reductions in both SO_2 and NO_x emissions, was conducted to examine the concurrent responses of fine particles, precipitation acidification, and nitrogen deposition. The simulated ambient gases and particle concentrations were extracted from the first layer at an approximately 25 m aboveground.

The anthropogenic emissions were derived from the Multi-resolution Emission Inventory for China (MEIC, available at www.meicmodel.org) database and those in surrounding countries from MIX (23). MEIC emissions database used in this study covers four anthropogenic sources at a monthly temporal resolution: power plants, industrial, residential, and transportation sectors. The biogenic emissions importing into WRF-Chem were calculated online using MEGAN (Model of Emissions and Gases from Nature) (24). As aforementioned, the gridded NH_3 emissions used in simulation were provided from the PKU-NH_3 model. Our inventory shows that intense emission mainly concentrates in northern China, Sichuan Basin and parts of Xinjiang province, and seasonally peaks in spring and summer due to intensive agricultural activities and relatively high air temperature. We considered diurnal variation in the NH_3 emissions with much higher fractions (~ 80%) in the daytime according to other studies (25-27).

Detailed model configuration is shown as following. The model domain was defined as China and its surrounding area with a 30 × 30 km horizontal resolution, as shown in Fig. S2. There were 21 terrain-following vertical layers from ground level to top pressure of 50 hPa, including 7 and half levels in the lowest 1 km or so. CBM-Z chemical mechanism was used for modeling photochemical reactions of gas phase species (28); MOSAIC aerosol module was used to treat aerosol nucleation, growth and related thermodynamic equilibrium (29); The Lin et al. microphysics and Grell 3D convection parameterizations were selected to simulate precipitation-related processes, including in-cloud scavenging of aerosols and trace gases (30). The below-cloud scavenging of aerosols by impaction/interception and traces gases by mass transfer have been treated in WRF-Chem following methods in Easter et al. (31). The calculation of dry deposition velocities was based on the methods of Wesely (32)

for trace gases, and Binkowski and Shankar (33) for aerosols. The initial and boundary meteorological conditions were derived from 6-h National Centers for Environmental Prediction reanalysis data (FNL, available at https://rda.ucar.edu/datasets/ds083.2/#!access). We used MODIS (Moderate Resolution Imaging Spectroradiometer, https://modis.gsfc.nasa.gov/data/) data to specify the land cover type, green vegetation fraction, and leaf area index in the domain following the methods of Li et al. (34), who have shown a better performance for meteorological simulation with these updated land surface parameters. To better reproduce wind-blown dust aerosols, we redefine the natural dust source in WRF-Chem as Gobi, sand, loess and mixed soil following Huang et al. (9). Besides, heterogeneous formation pathways of sulfate and nitrate were incorporated in the model based on Huang et al. (9). We assumed hydrated/deliquesced aerosol surfaces involved as the reactive media in the heterogeneous formation of particulate sulfate. Following Huang et al. (35), an apparent reaction rate expression was used to treat the oxidation of gaseous SO_2 on aerosol surfaces under high humidity conditions. The uptake coefficient γ, serving as a proxy of the magnitude of heterogeneous uptake, was assumed to depend linearly on RH (RH ≥ 50%) following Wang et al. (36) and Zheng et al. (37),

$$\gamma_{RH} = \gamma_{50\%} + \frac{(RH - 50\%)}{50\%} \cdot (\gamma_{100\%} - \gamma_{50\%}) \quad (2)$$

in which $\gamma_{100\%}$ and $\gamma_{50\%}$ were equal to 2.0×10^{-4} and 2.0×10^{-5}, specified as the upper and lower limits of uptake coefficients at the RH range of 100%−50%.

To enable the simulation of precipitation acidity, we developed a diagnosis program coupled with the WRF-Chem wet deposition module to calculate precipitation pH. First, the simulated wet deposition of gases and aerosol compounds through wet scavenging processes (e.g., in-cloud rainout and below-cloud washout) was accumulated within each grid during rainfall. The precipitation pH was then calculated with iterative methods to meet charge conservation and dissociation equilibrium in aqueous solution. The chemical species determining precipitation acidity involved SO_4^{2-}, HSO_4^-, NO_3^-, Cl^-, HCO_3^-, CO_3^{2-}, NH_4^+, Ca^{2+}, Mg^{2+}, Fe^{3+}, Mn^{2+}, and Na^+. Among these ions, SO_4^{2-}, HSO_4^-, NO_3^-, NH_4^+, Cl^- and Na^+ were determined from wet scavenging and subsequent dissociation equilibrium incorporated in our developed pH-diagnosis program. HCO_3^- and CO_3^{2-} concentrations in solution were resolved according to the effective henry constant for CO_2 and first and second dissociation equilibrium with a constant gas-phase CO_2 mixing ratio equal to 400 ppm in ambient air. Considering that Ca^{2+}, Mg^{2+}, Fe^{3+}, and Mn^{2+} could not simulated in the wet scavenging module, we gave their mass fractions in mineral particles when calculating precipitation acidity. They were 10%, 4%, 0.5% and 0.5% in fine-mode mineral particles, and 30%, 8%, 0.5% and 0.5% in coarse-mode mineral particles, respectively (35, 38, 39).

Observation datasets. We conducted evaluation of simulated $PM_{2.5}$ mass concentrations and the three major ions (sulfate, nitrate, and ammonium) against daily

observations collected at 35 monitoring stations across China during JJA and DJF of 2015. The information of observations is shown in Fig. S2 and Table S3, 4. Details on sampling methods and chemical analyzes for these datasets were shown in Wen et al. (40), Cao et al. (41), Ding et al. (42), Wang et al. (43), Wang et al. (44), and Huang et al. (45). To validate the simulated precipitation acidity, we used a national acid rain monitoring network developed by China Meteorological Administration (CMA, http://www.cma.gov.cn/). This network operated from 1992 with the total number of the stations increasing from 81 initially to more than 300 now. The sampling methods and data quality control were shown in Tang et al. (46). The wet deposition data of precipitation ions including sulfate, nitrate, and ammonium were provided by the yearly reports issued by the Acid Deposition Monitoring Network in East Asia (EANET, http://www.eanet.asia/). As one of the participator of EANET, China conducts regular acid deposition monitoring at four cities, namely Xi'an, Chongqing, Xiamen and Zhuhai. The surface NH_3 concentrations were collected from a nationwide NH_3 observation network with passive NH_3 diffusive samplers (Analysts, CNR-Institute of Atmospheric Pollution, Roma, Italy) over China (47).

We also used satellite observations of atmospheric SO_2 and NO_x column concentrations to present their inter-annual trends over China. The SO_2 and NO_x vertical column densities were derived from measurements by ozone monitoring instrument (OMI) onboard NASA Aura (available online at: https://disc.sci.gsfc.nasa.gov/ and http://www.temis.nl/index). Tropospheric vertical column densities of NH_3 were derived from the measurements of Infrared Atmospheric Sounding Interferometer (IASI) onboard MetOp-A (48-50).

Model evaluation. First, we compared the simulated surface NH_3 concentrations with nationwide measurements on a seasonal level. As shown in Fig. S3, WRF-Chem can capture the magnitude and spatial patterns of ground NH_3 concentrations, which reached more than 20 μg m^{-3} during JJA in Northern China, known as the hotspot of NH_3 emissions across China. The NH_3 concentrations during JJA were generally 2−3 times larger than those during DJF. The simulated NH_3 vertical column densities (VCDs) by using our inventory in WRF-Chem agreed well with observations from satellite on the magnitude and the spatial distribution (Fig. S3 C-D). Clearly, hotspots of NH_3 VCDs, as high as 30×10^{15} molecules/cm^2, were mainly found in North China Plain, coinciding with high loadings of NH_3 emissions in the region. Moreover, we also evaluated the model by using the in-situ observations of HNO_3 concentrations in Beijing (51), which shows a good agreement between the simulation and measurement (Average values: 0.21 vs. 0.36 μg m^{-3} in winter; 4.0 vs. 3.1 μg m^{-3} in summer).

Our simulation well reproduced the seasonal and spatial variation of $PM_{2.5}$ concentrations over China in 2015 (Fig. S4 and Table S5). The simulated $PM_{2.5}$ concentrations generally agreed with observations, with normalized mean biases (NMBs) within ± 10% and correlation coefficients of 0.65. More than 80% of model results were within a factor of two compared to the observations (FAC2 > 80%). Both

observations and simulations showed overall higher levels of $PM_{2.5}$ pollution in winter than in summer. Spatially, the seasonal mean concentrations reached as high as 100 μg/m^3 in Northern China in DJF, and decreased to 60 μg/m^3 in JJA.

The simulated inorganic $PM_{2.5}$ chemical compositions of interest (sulfate, nitrate, and ammonium) were compared with daily observations in Fig. S4 and Table S5. The simulated $PM_{2.5}$ sulfate agreed well with observations in JJA, with a low NMB (6.0%) and a large fraction (82%) of model results within a factor of two with observations. But they were somewhat underestimated in the Northern China (−22.9%) and Southern China (−21.6%) in DJF, which could be partly attributable to missing mechanisms of secondary sulfate formation in the current model (52) or the model limitation in reproducing atmospheric boundary layer structure (53). The nitrate was well captured by WRF-Chem with low NMBs (3.8% and −8.9%) and large FAC2 (> 60%) in both JJA and DJF. Only in DJF, the simulated nitrate were underestimated in the Northern China by −2.7 μg m^{-3}, and overestimated in the Sichuan Basin (2.6 μg m^{-3}) (Table S5). In general, both observation and simulation demonstrate that the concentrations of nitrate were much higher in DJF, with a seasonal average range of 10−20 μg m^{-3} in the Northern China, Southern China, and Sichuan Basin.

Considering the importance of nitrate in the reductions of $PM_{2.5}$ by NH_3 emission control, we used the China Air Quality Standard for daily $PM_{2.5}$ concentrations (75 μg m^{-3}) to define pollution and clean events, and then compared the model performance of nitrate separately under these conditions in DJF. It shows that the simulated nitrate concentrations were close to the observations in Northern China, Southern China, and Sichuan Basin, and the model can reproduce the gap of observed nitrate between these two conditions (Fig. S5A). For ammonium, the simulations were in overall good agreement with the measurements, showing the mean biases (MBs) of 0.4 μg m^{-3} in JJA and −0.7 μg m^{-3} in DJF. Generally, the systematic underestimation of particulate matter during wintertime is likely associated with the model limitation in reproducing atmospheric boundary layer structure (calms winds, temperature inversion and weak turbulence) during the stagnant days (53-55). Moreover, the uncertainties of precursor emissions and meteorology fields could contribute to the biases of simulated SNA.

According to the simulations results, these biases could not change our major findings. First, sulfate was not sensitive to NH_3 emissions reductions because of its low vapor pressure and thermodynamic stable nature, so the bias of sulfate in DJF (−17.0%) had few effect on $\Delta PM_{2.5}$. The effect of ammonium nitrate bias was tested by running an aerosol thermodynamic model (ISORROPIA-II) under typical winter conditions ($[SO_4^{2-}]$=12 μg m^{-3}, $[NO_3^-]$=12 μg m^{-3}, $[NH_4^+]$=8 μg m^{-3}, $[NH_3]$=5 ppb, $[HNO_3]$=1 ppb, RH=50%, T=275 K; the model configuration of ISORROPIA-II can be found Liu et al., (51)). It shows that the nitrate bias (−8.9%) would introduce the bias of −8% in the mass reductions of nitrate caused by NH_3 emission control. Moreover, we estimated that these negative biases of particulate nitrate and ammonia during wintertime would give rise to the bias of the annual nitrogen deposition only 3%.

The accumulated precipitation (only consider rainfall in this study) was evaluated against observations from national acid rain network (Fig. S6). The scatter plots demonstrated a good performance of precipitation simulation, with general NMBs of 12% and −19% in JJA and DJF, respectively. Influenced by East Asia summer monsoon, precipitation in China demonstrated typical seasonal distribution. The seasonal accumulated amounts peaked in summer, reaching above 500 mm in most of eastern stations but fewer than 100 mm in winter. We compared volume-weighted mean precipitation pH with observations on a seasonal basis. The percentages of errors within ± 0.5 / 1.0 units between simulation and observation were 45 / 70% in JJA and 40 / 64% in DJF, respectively. They showed that acid rain pollution with pH < 5.6 was mainly concentrated in Southern China, while seldom any acid rain area was found in West China because of the neutralization of alkaline dust aerosols and much fewer anthropogenic emissions.

Economic assessment. We conducted an integrated economic analysis on the potential NH_3 emission reductions in order to determine a cost-effective control strategy over China. First, we estimated the economic cost of NH_3 abatement options in livestock manure management following the methods of the Greenhouse gas – Air pollution INteractions and Synergies model (GAINS, available at http://gains.iiasa.ac.at.).

As described in the report by Klimont and Winiwarter (56), the GAINS model considers three types of expenditures, that is, investments (I), fixed operating costs (FO, maintenance) and variable operating costs (VO). Investments include all the expenditure before the start-up of an abatement option, e.g., construction, engineering and consulting. The GAINS model calculates the investment as a function of the average farm size (*AFS*, i.e., the average number of animal places on a large farm). We used the following function to estimate the investment in the manure storage stage,

$$I_{i,k} = ci^{f}_{i,k} \cdot \frac{st_i}{12} \cdot mp_i \cdot ar_i + \frac{ci^{v}_{i,k}}{AFS_i} \tag{3}$$

where *i, k* represent livestock category and abatement technique, respectively; *st* represents manure storage time; *mp* represents manure production of a single animal per year; *ar* represents production cycles per year. The *AFS* and *ar* values were derived from Kang et al. (2), who gave the information for major livestock animals in China. Other parameters used in the function were available in on-line GAINS or the report. The investments were then annualized using following equation,

$$I_{i,k}^{an} = I_{i,k} \cdot \frac{(1+q)^{lt_k} \cdot q}{(1+q)^{lt_k} - 1} \tag{4}$$

where *q* represents the interest rate (4% in GAINS); *lt* represents the lifetime of abatement technique (10−15 years). Annual fixed operating cost FO was estimated as the percentage (*per*) of the total investments. The value of *per* was set to 0.05%

according to GAINS.

$$FO_{i,k} = I_{i,k} \cdot per_{i,k} \quad (5)$$

Variable operating costs VO were calculated by the product of the quantity (Q, like labour and animal feed) of a certain extra supply for a specific abatement option (k) and its unit price (c). In this work, we considered VO for low protein feeding, treatment of manure in animal house, and low ammonia application in arable land.

$$VO_{i,k} = \sum_{p} (Q_{i,k} \cdot c_{i,k}) \quad (6)$$

The unit labour cost was set to 35 Chinese yuan (5.1 US$) / per hour according to the national averaged salary for individual person given by China Statistic Yearbook for 2016 (http://www.stats.gov.cn/tjsj/ndsj/). Other relevant parameters used in the calculation of FO and VO were obtained from GAINS. The annual total cost (AC) of individual abatement cost was the product of the number of livestock animals (N) and sum of these three parts:

$$AC_k = \sum_{i} (I^{an}{}_{i,k} + FO_{i,k} + VO_{i,k}) N_i \quad (7)$$

Besides livestock sector, GAINS considers improvement of urea fertilizer application or its substitution. GAINS developers (56) reported those abatement costs ranging between 1.0−2.0 EUR per kg removed NH_4-N for European countries. Here, The median value of 1.5 EUR (1.7 US$) per kg removed NH_4-N was used in our study to estimate the cost of improvement of nitrogen fertilizer application (avoiding over-fertilization and improving nitrogen use efficiency).

Then, we conducted the economic assessment on the effects of NH_3 emission control, including the health effects related to $PM_{2.5}$ pollution and ecosystem effects related to acid rain and nitrogen deposition. We estimated the premature mortality attributable to $PM_{2.5}$ exposure by using an exposure-response function that has been applied in many previous studies on the global and national scales (57-60). Following Liu et al. (57), four specific diseases related with premature mortality due to $PM_{2.5}$ were considered, namely ischemic heart disease, cerebrovascular disease (including ischemic stroke and hemorrhagic stroke), chronic obstructive pulmonary disease, and lung cancer. The baseline mortality rates from these four diseases were collected on the nation scale in datasets of Global Burden of Disease (GBD) study for 2013, http://ghdx.healthdata.org/global-burden-diseasestudy-2013-gbd-2013-data-downloads). The gridded $PM_{2.5}$ concentrations and population were required in the calculation of premature mortality due to $PM_{2.5}$ pollution. The former was provided by averaging the model results in the simulation period (JJA and DJF). The population dataset (1 km × 1 km) for China was provided by National Science and Technology Infrastructure Project: Data Sharing of Earth System Science (www.geodata.cn) and rescaled to the simulation domain with a resolution of 30 km × 30 km. After calculating the one-year premature mortality attributable to $PM_{2.5}$ exposure, we used the value of a statistical life (VOSL) to derive corresponding economic effect. The

VOSL values have been given in many previous literatures (61-65). For instance, Wang et al. (64) conducted a contingent valuation study in Chongqing, China in 1998 and showed the VOSL of approximately US$ 34,750. In this study, we used the value of 0.86 million Chinese Yuan (USD to Chinese Yuan exchange rate was equal to 6.8) derived from a meta-analysis study for China (66).

The studies on the quantification of damage of precipitation acidification to ecosystems were quite limited. Singh and Agrawal (67) exposed wheat plants to simulated precipitation pH in house and found their yields decreasing by more than 10 percent at pH below 5.0. Evans et al. (68) found that the yields of soybeans decreased with increased precipitation acidity in America. Feng et al. (69) investigated the effects of acid rain on agriculture and forestry in southern China in 1990s. They conducted both field investigation and laboratory simulations to quantify the response of China's crop and forest yields to precipitation pH. Their results assisted the Chinese government to guide the control on acid rain pollution. Bases these studies, we quantitatively assessed the economic loss of crop and forestry due to enhanced precipitation acidification attributable to NH_3 emission control. In this approach, the reductions in crop yield and forestry varied with different pH intervals and plant species. We considered four crop species including wheat, cotton, soybean, and vegetable in the assessment. For instance, when acid rain pH values are 5.0−5.6, 4.5−5.0, and <4.5, the corresponding decreases in vegetable yield were 3, 5, and 10 percent, respectively (69). Then, the economic loss of crop at each grid was estimated based on the actual yield, the percent reductions due to acid rain, and price per unit yield. The actual annual yield of different crops on the province scale and the price per unit were obtained from Chinese Agricultural Yearbook (70). A land cover dataset (GLC-2000 China, http://forobs.jrc.ec.europa.eu/products/glc2000/products.php) was used to allocate the province-level crop production to the model grids belonging to cropland. Similarly, the decline in forestry (timber products) caused by acid rain and associated economic loss were also estimated based on above methods. Only two forest species, namely Masson Pine and Chinese fir, were considered in the estimation.The non-timber forest products like carbon sequestration, watershed protection, and recreation are likely to be high. Their economic values were assumed to be five times that of the timber according to previous reports (71). The total loss of forestry was the sum of reductions in timber and non-timber products.

The economic impact of nitrogen deposition was estimated based on the exceedance of nitrogen critical load and a unit damage cost for ecosystems provided by an integrated report for the costs and benefits of nitrogen in Europe (72). They estimated a cost of 2.3 Euro (2.7 US$) per kg NH_3-N for acidification and eutrophication of ecosystems. We adopted this value to calculate the potential benefit from reduced nitrogen deposition due to NH_3 emission control in those areas receiving critical load exceedance of nitrogen. We should point out that the estimation may be subjected to large uncertainties, and the results need to be evaluated in future studies.

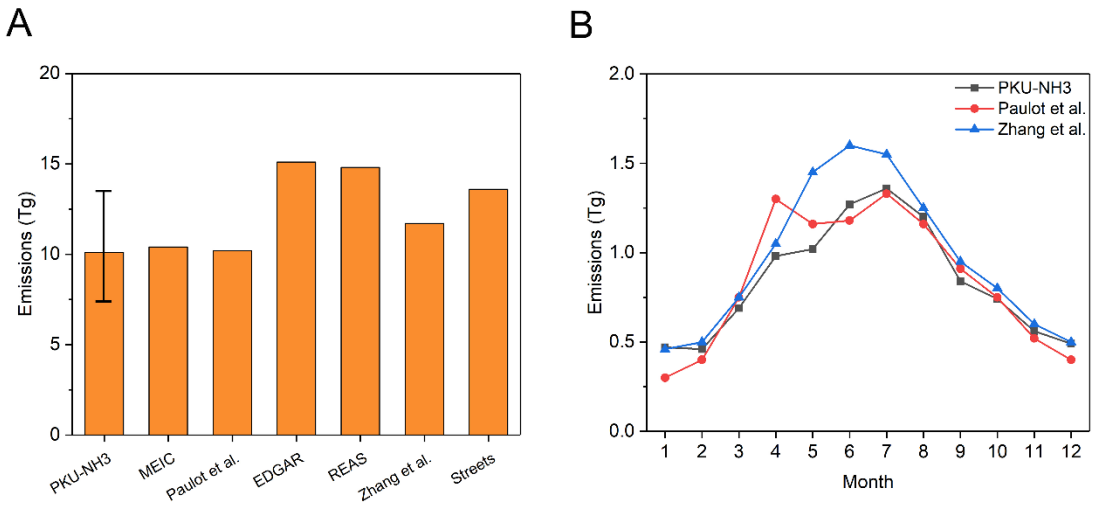

Fig. S1. Evaluation of NH_3 emission inventory (PKU-NH_3) used in this study. (A) Comparison of the national emission estimate in PKU-NH_3 with other inventories. The vertical bar denotes the uncertainty range; (B) Comparison of the estimated monthly emissions with other studies based on top-down methods.

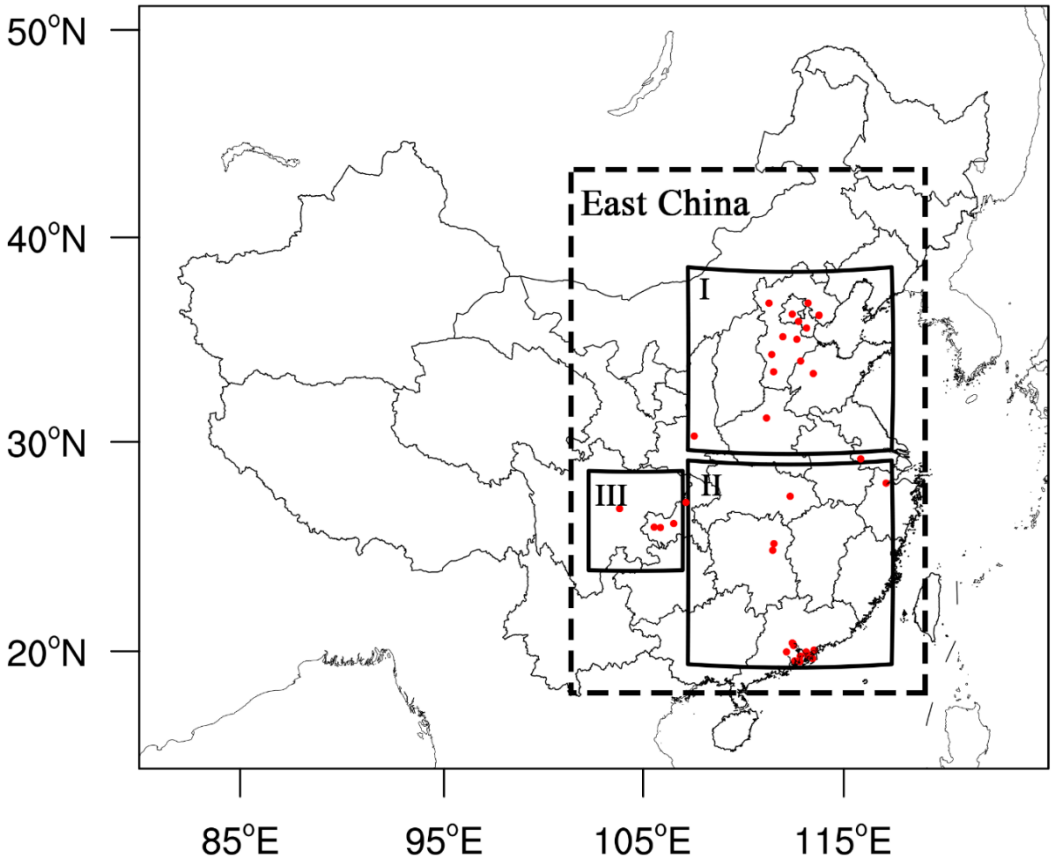

Fig. S2. WRF-Chem simulation domain and three regions of concern: (I) Northern China, (II) Southern China, and (III) Sichuan Basin. The red scatters denote the observation stations used to evaluate the model performance of $PM_{2.5}$ inorganic chemical constituents.

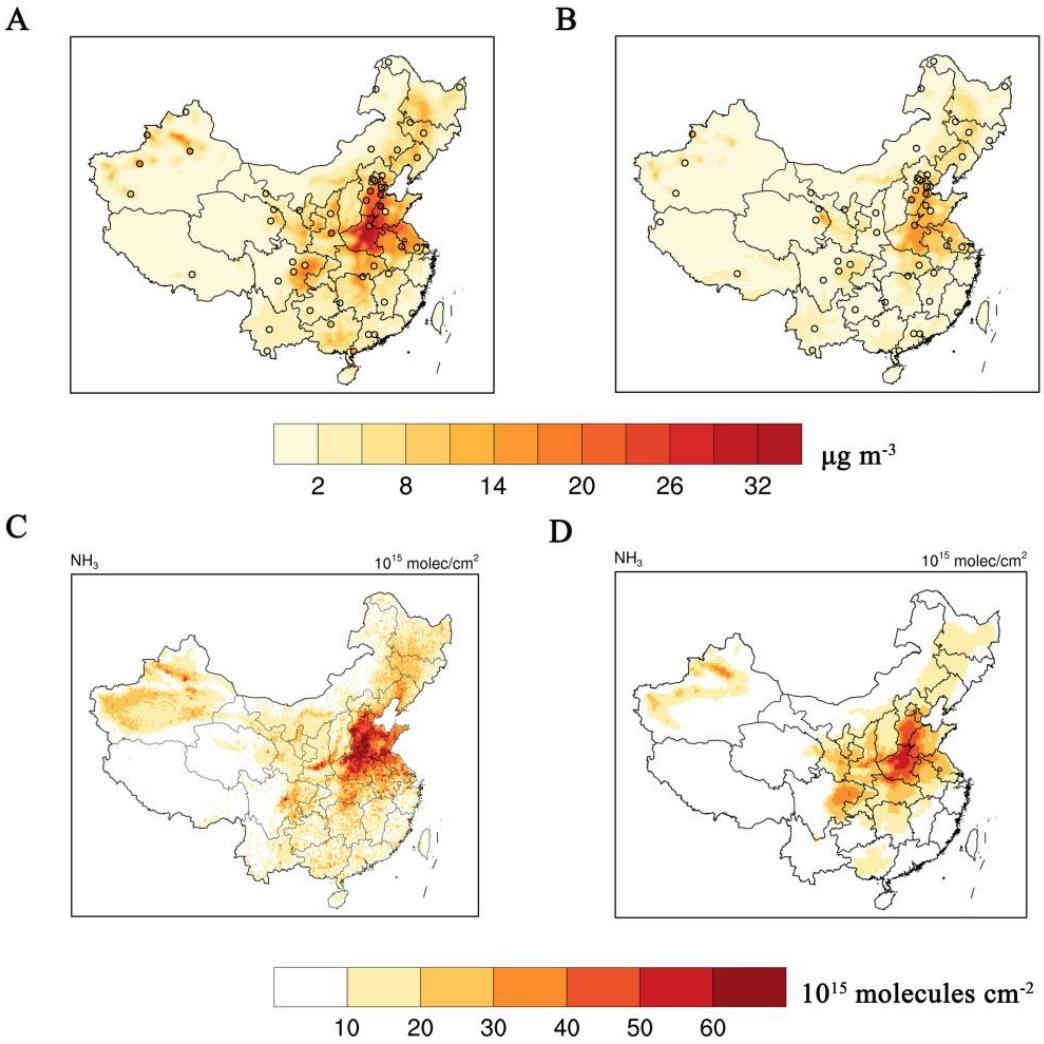

Fig. S3. Evaluation of simulated NH_3 concentrations against nationwide surface NH_3 measurements (A-B) and satellite retrievals (C-D). We present spatial patterns of mean vertical column densities of NH_3 derived from IASI daytime measurements (C) and WRF-Chem simulation with our inventory (D) during JJA, 2015. Wintertime result (DJF) of NH_3 columns is not used for evaluation because the signal of IASI is not sensitive to NH_3. NC, SC, and SCB denote Northern China, Southern China, and Sichuan Basin, respectively.

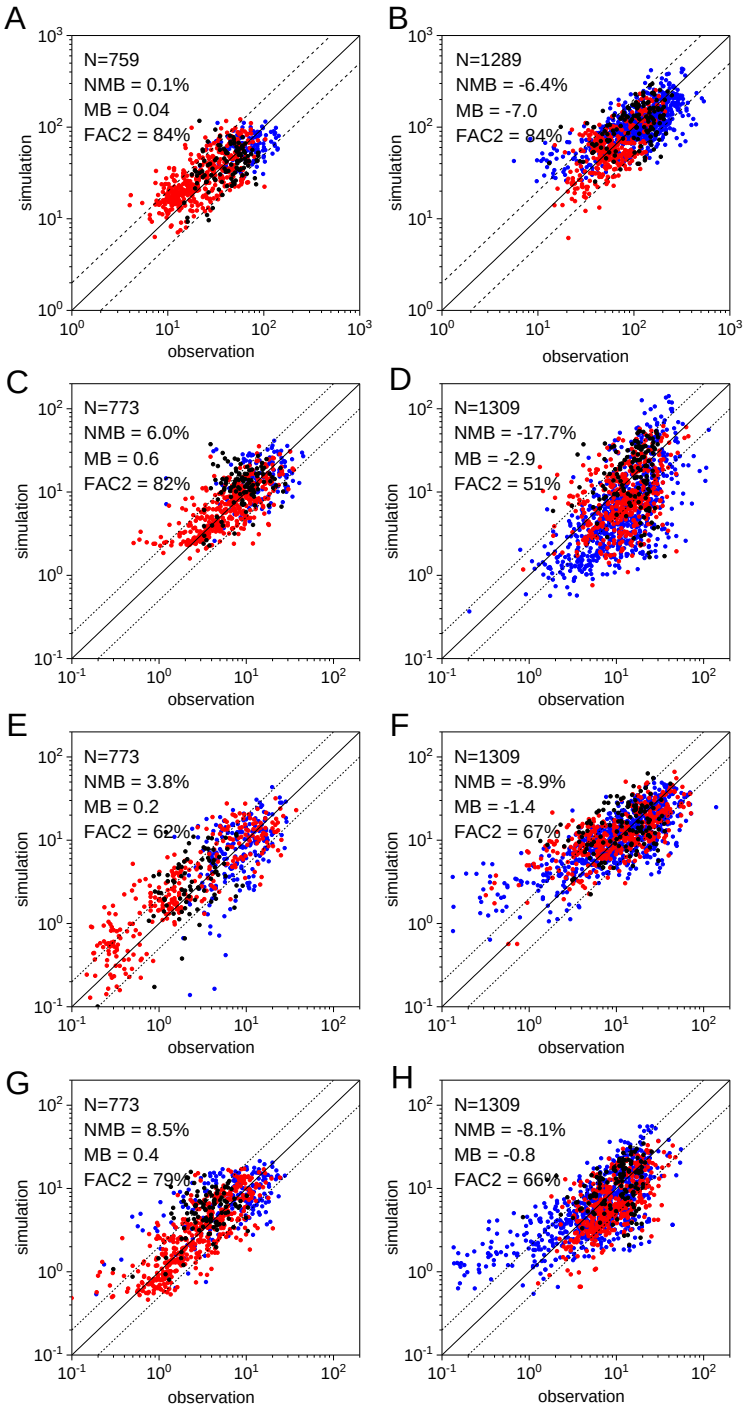

Fig. S4. Evaluation of simulated $PM_{2.5}$ concentrations (A−B) and three major chemical constituents (C−D, sulfate; E−F, nitrate; G−H, ammonium) against the daily observations at 37 stations during JJA (left column) and DJF (right column) of 2015. The colors denote the regions, i.e., blue is Northern China, red is Southern China, and black is Sichuan Basin. Three statistics index, normalized mean bias (NMB), mean bias (MB), and percentage of model results within a factor of two with observations (FAC2), are shown here for reference. The solid 1:1 line and two dashed 1:2 and 2:1 lines are shown.

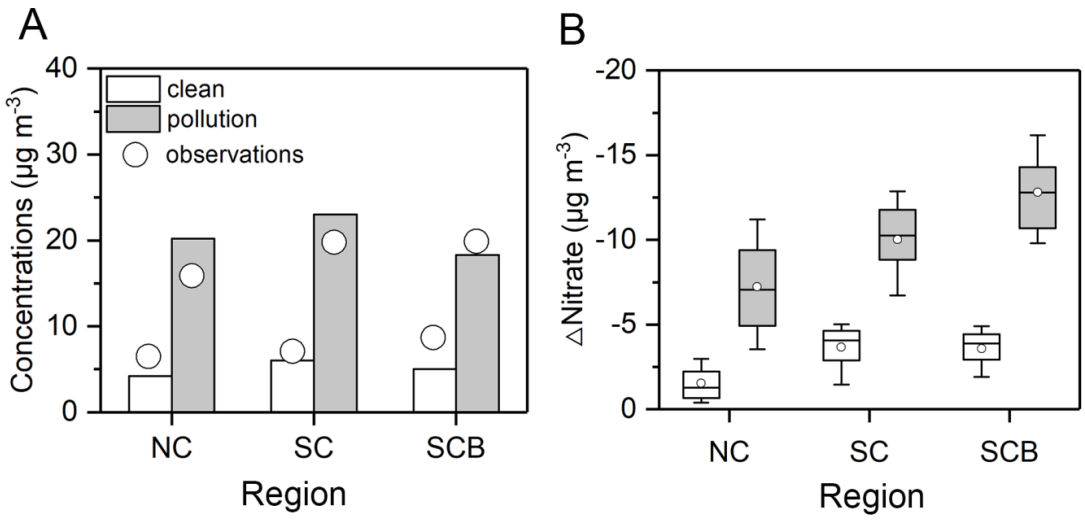

Fig. S5. (A) Evaluation of simulated nitrate concentrations against measured daily $PM_{2.5}$ at monitoring sites under pollution and clean conditions during wintertime. The China Air Quality Standard for daily $PM_{2.5}$ concentrations (75 μg m^{-3}) was used to distinguish pollution (> 75 μg m^{-3}) and clean days (< 75 μg m^{-3}). (B) Comparison of mass reductions in simulated particulate nitrate concentrations due to the NH_3 emission reduction under these two conditions. NC, SC, and SCB denote Northern China, Southern China, and Sichuan Basin, respectively. The box and whisker plots are drawn for the 10th, 25th, 50th, 75th and 90th percentiles. The black circles denote the mean values.

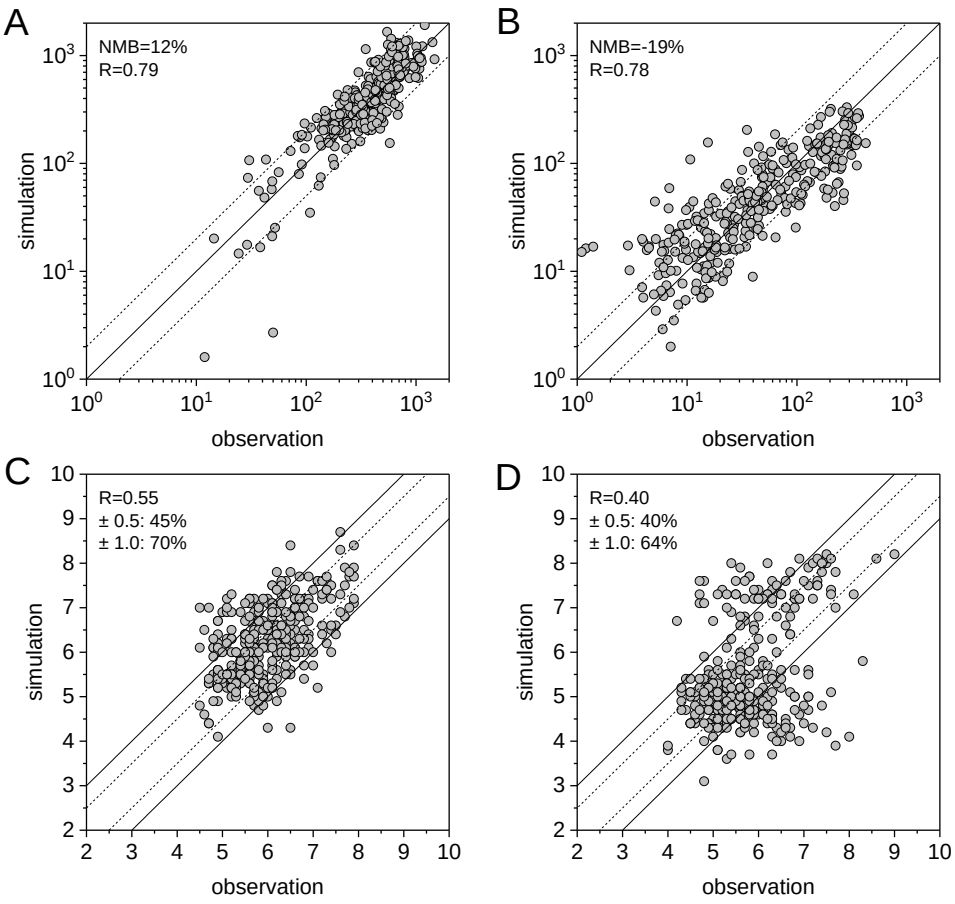

Fig. S6. Comparison of simulated seasonal precipitation amounts (A-B) and precipitation-weighted mean pH values (C-D) with observations from China acid rain network during JJA (left column) and DJF (right column) of 2015. The solid 1:1 line and two dashed 1:2 and 2:1 lines are shown in the comparison of precipitation, and the two dashed ± 0.5 lines and two solid ± 1.0 lines are shown in the comparison of pH.

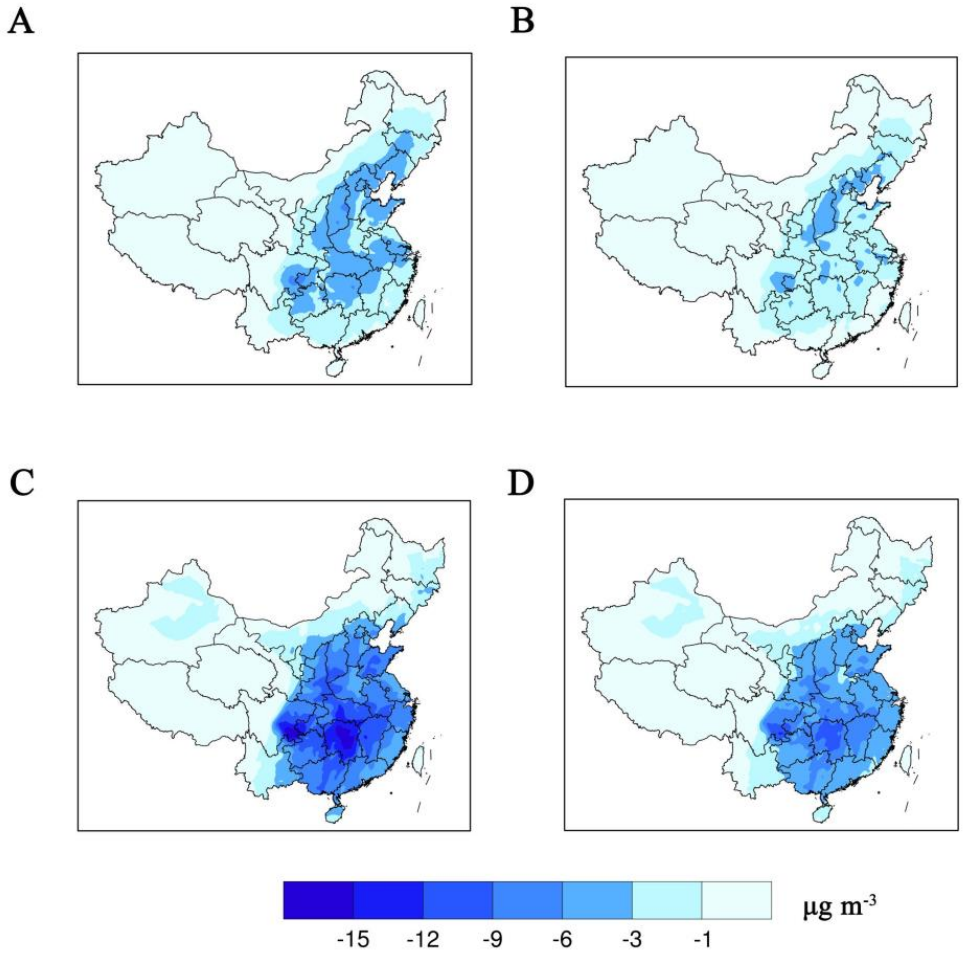

Fig. S7. Reductions in $PM_{2.5}$ (left column) and nitrate (right column) concentrations due to a 50% NH_3 emission reduction during JJA (A-B) and DJF (C-D).

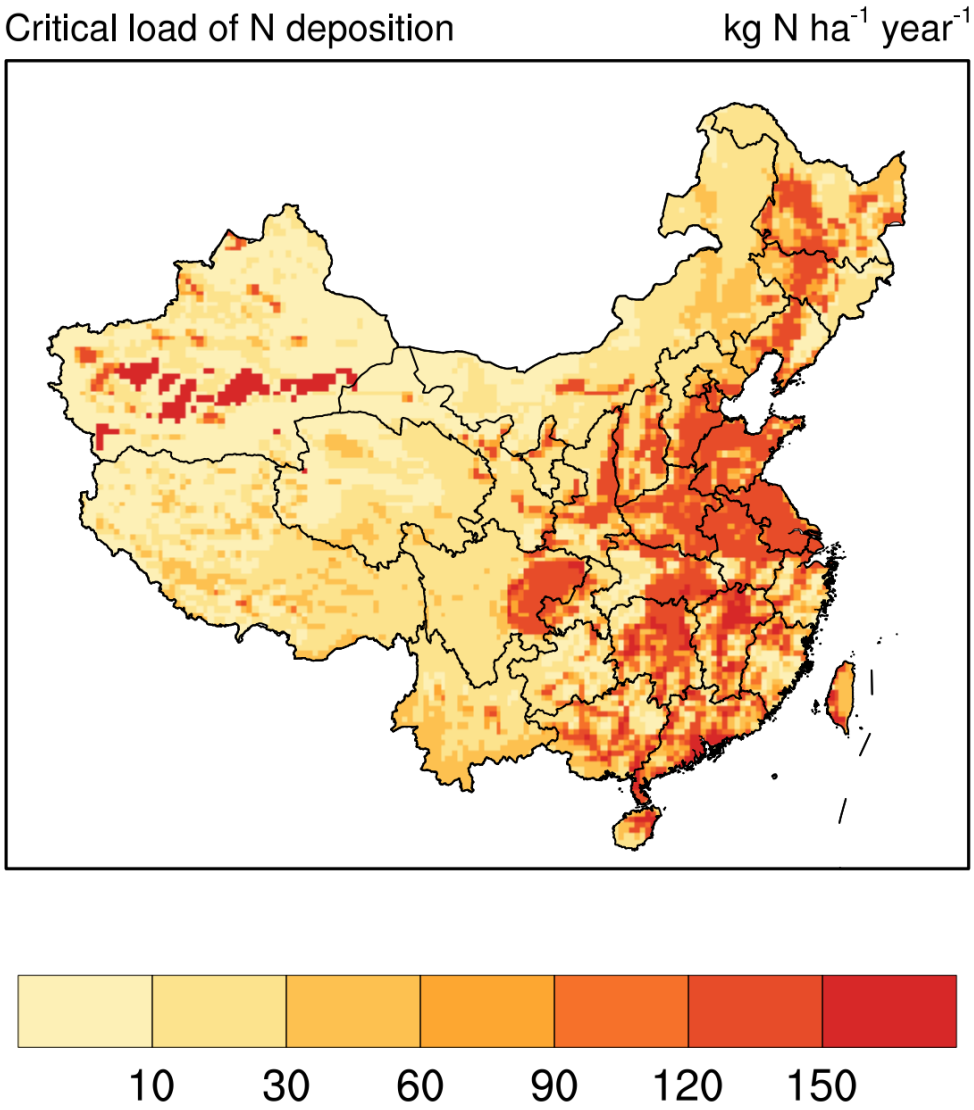

Fig. S8. The critical loads of nitrogen deposition over China. The map were developed by Posch et al. (73) based on steady state mass balance method.

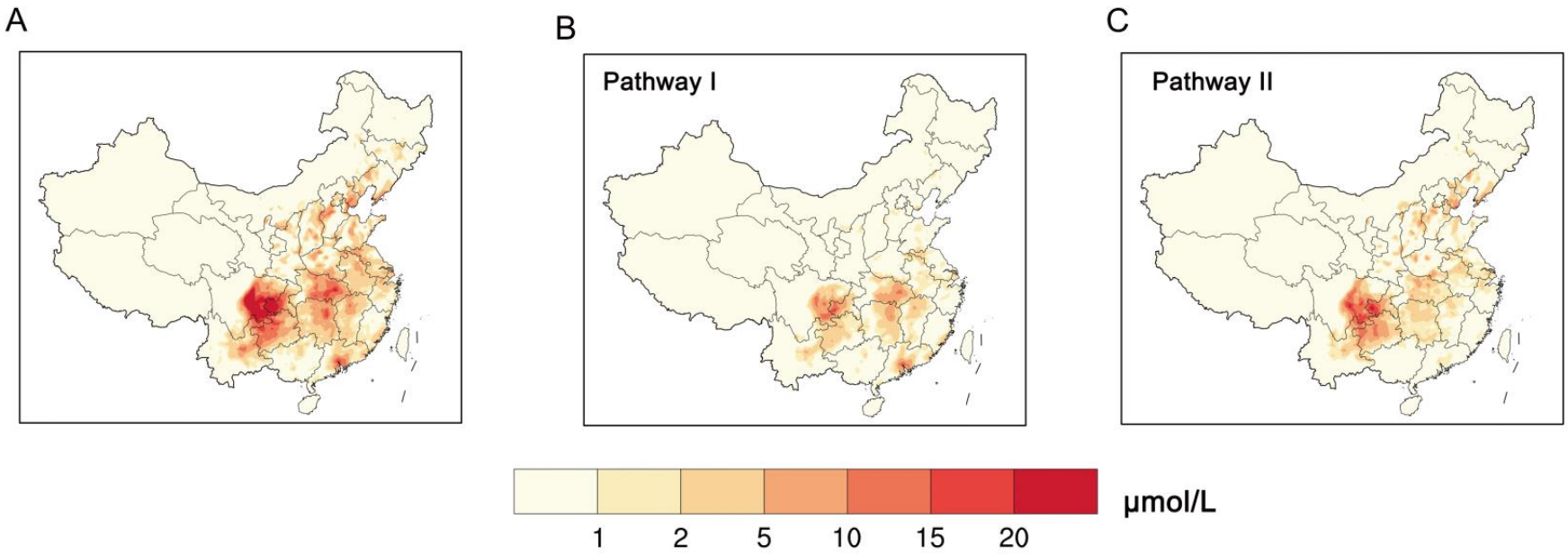

Fig. S9. Increased concentrations of hydronium ion in precipitation due to NH_3 emission reductions. A represents the total enhancement of precipitation acidity due to NH_3 reductions. B and C represent the two major pathways of the enhancement. Pathway I links to decreased wet scavenging of gas-phase NH_3 in air; Pathway II links to increase in wet scavenging of bisulfate due to the transition of ammonium sulfate to ammonium bisulfate.

Table S1. The NH_3 emission control options and corresponding reduction efficiency (%).

Abatement option	Application processes	Reduction efficiency (η)	Sources
Avoiding over-fertilization	Synthetic fertilizer application	> 20%	Ju et al. (12) and Wu et al. (13)
Deep application of fertilizers	Synthetic fertilizer application	~50%	Estimated by Huang et al. (1)
Low crude protein feed	Whole manure management chain	10−40%	Hou et al. (19)
Using deep litter in floor and regular washing	Manure in house	20−50%	Klimont and Brink (74), Wang et al. (17)
Covering solid and slurry manure	Manure storage	> 60%	Wang et al. (17) and Hou et al. (19)
Incorporation or plough after spreading	Field application of manure	40−80%	Sommer and Hutchings (75)

Table S2. Comparison of NH_3 EFs for major livestock animal (kg (1000 kg N released)$^{-1}$ year^{-1}) and fertilizer (kg (1000 kg N applied)$^{-1}$ year^{-1}) in China before and after a 50% emission reduction with those of USA, Europe and the Global average for developed countries.

Source	China[a] (present)	China[a] (future)	USA[b]	Europe[c]	Global[d]
Swine	636	232	263	537	398
Beef cattle	423	172	276	224	230
Sheep	337	156	205	90	50
Poultry	750	340	440	480	480
Mineral nitrogen fertilizer	131	66	68	60	58−175

[a]The EFs in present conditions were derived from Huang et al. (1) and those in the future scenario were developed in this study.

[b]Values were derived from the National Emissions Inventory developed by U.S. Environmental Protection Agency (https://www.epa.gov/nei).

[c]Values were derived from European Environment Agency. (https://www.eea.europa.eu/) and the inventory developed by Paulot et al. (3).

[d]Values were derived from Bouwman et al. (76) and van Grinsven et al. (77).

Table S3. Description of observations sites in the three regions of concern.

Region	Site	ID	Number	Latitude	Longitude	Periods (Month, 2015))[a]
Northern China	Beijing	BJ	99	39.99	116.3	DJF, July
	Shijiazhuang	SJZ	70	38.34	114.54	DJF, July
	Tianjin	TJ	52	39.11	117.17	DJF
	Jinan	JN	124	36.68	117.18	DJF
	Langfang	LF	56	39.53	116.71	DJF
	Zhangjiakou	ZJK	54	40.75	114.89	DJF
	Tangshan	TS	80	39.64	118.17	DJF, July
	Baoding	BD	49	38.87	115.47	DJF
	Xingtai	XT	56	37.11	114.49	DJF
	Cangzhou	CZ	53	38.61	116.38	DJF
	Dezhou	DZ	55	37.44	116.38	DJF
	Xinglong	XL	54	40.40	117.59	DJF
	Xi'an	XA	144	34.23	108.88	DJF, JJA
	Zhengzhou	ZZ	28	34.8	113.52	January, July
Southern China	Nanjing	NJ	163	32.1	118.97	DJF, JJA
	Wuhan	WH	117	30.53	114.36	DJF, JJA
	Guangzhou	GZ	145	23.0	113.35	DJF, JJA
	Hangzhou	HZ	26	30.29	120.16	December
	Porto Exterior	PE	29	22.19	113.56	DJF, JJA
	Taipa Grande	TG	29	22.16	113.57	DJF, JJA
	Nanhai	NH	29	23.13	113.3	DJF, JJA
	Yuen Long	YL	29	22.45	114.02	DJF, JJA
	Tsuen Wan	TW	29	22.37	114.11	DJF, JJA
	Hok Tsui	HK	29	22.22	114.27	DJF, JJA
	Doumen	DM	31	22.23	113.3	January, July
	Qi'ao Island	QA	31	22.43	113.63	Jan., July
	Heshan	HS	42	22.73	112.93	January, July
	Modiesha	MDS	43	23.11	113.33	January, July
	University town	UT	68	22.59	113.98	DJF, JJA
	Dapeng	DP	31	22.63	114.41	January, July
	Changsha	CS	13	28.13	113.02	December
	Xiangtan	XGT	10	27.9	112.9	December
Sichuan Basin	Wanzhou	WZ	45	30.8	108.38	January, July
	Fuling	FL	48	29.75	107.27	January, July
	Shapingba	SPB	48	29.58	106.47	January, July
	Yubei	YB	56	29.62	105.5	January, July
	Chengdu	CD	56	30.63	104.07	January, July

[a]DJF and JJA denote the winter (December, January, and February) and summer months (June, July and August), respectively.

Table S4. Arithmetic mean concentrations of measured $PM_{2.5}$ and three major ions at individual monitoring sites in the regions of concern.

Region	Site	$PM_{2.5}$		Nitrate		Sulfate		Ammonium	
		JJA	DJF	JJA	DJF	JJA	DJF	JJA	DJF
Northern China	BJ	85.1	105.1	12.3	14.6	10.1	11.8	9.8	10.0
	SJZ	76.3	192.7	13.9	21.8	20.6	22.6	12.7	12.8
	TJ		131.2		14.8		14.3		8.5
	JN	71.5	123.4	8.7	19.0	17.2	16.6	11.1	8.2
	LF		148.1		14.4		14.8		8.1
	ZJK		78.9		6.3		8.0		2.9
	TS	77.7	121.1	12.4	15.8	14.2	18.9	11.5	6.8
	BD		168.8		16.4		16.0		9.0
	XT		145.2		17.8		19.0		11.6
	CZ		133.2		11.3		13.0		7.3
	DZ		136.5		20.1		19.3		11.2
	XL		54.9		7.7		6.3		3.7
	XA	70.2	173.4	7.0	27.9	13.6	23.7	4.0	11.5
	ZZ	85.1	167.8	13.0	25.7	23.2	21.0	13.2	17.9
Southern China	NJ	39.2	93.8	9.9	23.4	14.1	18.3	7.9	14.6
	WH	39.8	115.6	10.4	28.8	9.3	23.3	6.0	17.5
	GZ	24.2	48.6	2.1	8.1	6.7	9.2	2.8	7.8
	HZ		101.6		12.8		8.3		9.2
	PE	17.9	47.9	0.3	6.9	5.4	11.9	1.9	6.2
	TG	15.3	43.6	0.3	6.5	5.7	11.8	1.9	5.7
	NH	19.6	66.2	1.4	7.8	3.7	11.0	1.3	6.9
	YL	17.7	43.3	0.2	4.1	5.7	9.4	2.3	5.3
	TW			0.6	2.8	5.4	9.0	1.7	3.8
	HK	15.6	37.9	0.1	1.8	5.9	10.0	2.0	4.6
	DM	15.3	61.9	0.6	15.2	4.8	16.6	1.6	9.1
	QA	15.6	66.8	0.3	10.6	4.5	14.6	1.7	7.9
	HS	21.8	75.8	0.4	11.8	6.0	12.5	2.3	8.0
	MDS	23.1	65.0	1.1	8.2	6.3	12.5	2.5	7.1
	UT	19.3	54.0	0.4	6.4	4.8	10.6	1.9	6.0
	DP	16.0	45.4	0.3	3.1	5.1	11.9	1.9	5.2
	CS		99.5		7.2		17.7		7.8
	XGT		101.4		8.3		19.2		9.9
Sichuan Basin	WZ	26.4	84.4	1.4	9.4	8.9	16.6	3.4	9.8
	FL	47.9	120.5	2.3	14.9	11.0	17.5	4.2	12.1
	SPB	56.3	126.4	3.4	14.0	12.5	15.8	4.7	11.0
	YB	54.2	115.1	1.6	15.8	11.1	17.5	4.0	11.3
	CD	45.1	113.5	3.9	17.5	9.7	16.4	4.2	12.7

Table S5. Summary of the comparison of model results with the observations of $PM_{2.5}$ and its component concentrations in the three regions. NC, SC, and SCB denote Northern China, Southern China, and Sichuan Basin, respectively.

Region	Variables	JJA				DJF			
		Number	MB	NMB	FAC2	Number	MB	NMB	FAC2
NC	$PM_{2.5}$	230	−8.9	−12.2%	93.1%	744	−12.7	−9.8%	84.0%
	Nitrate	230	0.2	2.0%	60.6%	744	−2.7	−17.0%	68.8%
	Sulfate	230	0.5	3.0%	72.2%	744	−3.5	−22.9%	48.0%
	Ammonium	230	0.1	1.1%	65.2%	744	−0.3	−3.1%	64.4%
SC	$PM_{2.5}$	405	5.1	19.4%	86.0%	431	0.5	0.6%	85.6%
	Nitrate	419	0.1	2.0%	69.0%	446	−0.7	−4.9%	64.5%
	Sulfate	419	−0.2	−2.0%	91.0%	446	−2.8	−18.6%	54.6%
	Ammonium	419	0.0	0.3%	87.0%	446	−1.8	−17.8%	66.9%
SCB	$PM_{2.5}$	124	−1.8	−4.0%	83.0%	129	4.5	4.0%	83.1%
	Nitrate	124	0.9	31.2%	52.0%	129	2.6	17.5%	60.8%
	Sulfate	124	1.7	16.0%	81.0%	129	3.1	18.3%	62.3%
	Ammonium	124	1.4	34.0%	71.0%	129	0.8	6.6%	73.1%

References

1. Huang X, *et al.* (2012) A high-resolution ammonia emission inventory in China. *Global Biogeochem. Cy.* 26(1):GB1030.
2. Kang Y, *et al.* (2016) High-resolution ammonia emissions inventories in China from 1980 to 2012. *Atmos. Chem. Phys.* 16(4):2043-2058.
3. Paulot F, *et al.* (2014) Ammonia emissions in the United States, European Union, and China derived by high-resolution inversion of ammonium wet deposition data: Interpretation with a new agricultural emissions inventory (MASAGE_NH3). *J. Geophys. Res. Atmos.* 119(7):4343-4364.
4. Zhang L, *et al.* (2018) Agricultural ammonia emissions in China: reconciling bottom-up and top-down estimates. *Atmos. Chem. Phys.* 18(1):339-355.
5. Fu X, *et al.* (2015) Estimating NH3 emissions from agricultural fertilizer application in China using the bi-directional CMAQ model coupled to an agro-ecosystem model. *Atmos. Chem. Phys.* 15(1):745-778.
6. Kurokawa J, *et al.* (2013) Emissions of air pollutants and greenhouse gases over Asian regions during 2000–2008: Regional Emission inventory in ASia (REAS) version 2. *Atmos. Chem. Phys.* 13(21):11019-11058.
7. Streets DG, *et al.* (2003) An inventory of gaseous and primary aerosol emissions in Asia in the year 2000. *J. Geophys. Res. Atmos.* 108(D21).
8. Kim JY, *et al.* (2006) An investigation on NH3 emissions and particulate NH4+–NO3- formation in East Asia. *Atmos. Environ.* 40(12):2139-2150.
9. Huang X, *et al.* (2015) Direct Radiative Effect by Multicomponent Aerosol over China. *J. Climate* 28(9):3472-3495.
10. Cai GX, *et al.* (2002) Nitrogen losses from fertilizers applied to maize, wheat and rice in the North China Plain. *Nutr. Cycling Agroecosyst.* 63(2-3):187-195.
11. Cui Z, *et al.* (2018) Pursuing sustainable productivity with millions of smallholder farmers. *Nature* 555(7696):363-366.
12. Ju X, *et al.* (2009) Reducing environmental risk by improving N management in intensive Chinese agricultural systems. *Proc. Nat. Acad. Sci. U.S.A.* 106(19):8077–8078.
13. Wu Y, *et al.* (2018) Policy distortions, farm size, and the overuse of agricultural chemicals in China. *Proc. Natl. Acad. Sci. U.S.A.* 115(27):7010-7015.
14. Bai Z, *et al.* (2017) Livestock Housing and Manure Storage Need to Be Improved in China. *Environ. Sci. Technol.* 51(15):8212-8214.
15. Chadwick D, *et al.* (2015) Improving manure nutrient management towards sustainable agricultural intensification in China. *Agr. Ecosyst. Environ.* 209:34-46.
16. Bai Z, *et al.* (2016) Nitrogen, Phosphorus, and Potassium Flows through the Manure Management Chain in China. *Environ. Sci. Technol.* 50(24):13409-13418.
17. Wang Y, *et al.* (2017) Mitigating Greenhouse Gas and Ammonia Emissions

from Swine Manure Management: A System Analysis. *Environ. Sci. Technol.* 51(8):4503-4511.
18. Xinhua (2018) Low-protein feed can reduce China's dependence on soybean imports http://www.xinhuanet.com/english/2018-08/30/c_137430848.htm.
19. Hou Y, Velthof GL, & Oenema O (2015) Mitigation of ammonia, nitrous oxide and methane emissions from manure management chains: a meta-analysis and integrated assessment. *Global Change Bilo.* 21(3):1293-1312.
20. Chapman EG*, et al.* (2009) Coupling aerosol-cloud-radiative processes in the WRF-Chem model: Investigating the radiative impact of elevated point sources. *Atmos. Chem. Phys.* 9(3):945-964.
21. Grell GA*, et al.* (2005) Fully coupled "online" chemistry within the WRF model. *Atmos. Environ.* 39(37):6957-6975.
22. Fast J*, et al.* (2009) Evaluating simulated primary anthropogenic and biomass burning organic aerosols during MILAGRO: implications for assessing treatments of secondary organic aerosols. *Atmos. Chem. Phys.* 9(16):6191-6215.
23. Li M*, et al.* (2017) MIX: a mosaic Asian anthropogenic emission inventory under the international collaboration framework of the MICS-Asia and HTAP. *Atmos. Chem. Phys.* 17(2):935-963.
24. Guenther A*, et al.* (2006) Estimates of global terrestrial isoprene emissions using MEGAN (Model of Emissions of Gases and Aerosols from Nature). *Atmos. Chem. Phys.* 6(11):3181-3210.
25. Asman WA (2001) Modelling the atmospheric transport and deposition of ammonia and ammonium: an overview with special reference to Denmark. *Atmos. Environ.* 35(11):1969-1983.
26. Paulot F*, et al.* (2016) Sensitivity of nitrate aerosols to ammonia emissions and to nitrate chemistry: implications for present and future nitrate optical depth. *Atmos. Chem. Phys.* 16(3):1459-1477.
27. Zhu L*, et al.* (2015) Global evaluation of ammonia bidirectional exchange and livestock diurnal variation schemes. *Atmos. Chem. Phys.* 15(22):12823-12843.
28. Zaveri RA & Peters LK (1999) A new lumped structure photochemical mechanism for large-scale applications. *J. Geophys. Res. Atmos.* 104(D23):30387-30415.
29. Zaveri RA, Easter RC, Fast JD, & Peters LK (2008) Model for Simulating Aerosol Interactions and Chemistry (MOSAIC). *J. Geophys. Res. Atmos.* 113(D13):D13204.
30. Lin Y-L, Farley RD, & Orville HD (1983) Bulk Parameterization of the Snow Field in a Cloud Model. *J. Appl. Meteorol.* 22(6):1065-1092.
31. Easter RC*, et al.* (2004) MIRAGE: Model description and evaluation of aerosols and trace gases. *J. Geophys. Res. Atmos.* 109(D20).
32. Wesely M (1989) Parameterization of surface resistances to gaseous dry deposition in regional-scale numerical models. *Atmos. Environ.*

23(6):1293-1304.
33. Binkowski FS & Shankar U (1995) The Regional Particulate Matter Model: 1. Model description and preliminary results. *J. Geophys. Res. Atmos.* 100(D12):26191-26209.
34. Li M*, et al.* (2014) Improving mesoscale modeling using satellite-derived land surface parameters in the Pearl River Delta region, China. *J. Geophys. Res. Atmos.* 119(11):6325-6346.
35. Huang X*, et al.* (2014) Pathways of sulfate enhancement by natural and anthropogenic mineral aerosols in China. *J. Geophys. Res. Atmos.* 119(24):14,165-114,179.
36. Wang Y*, et al.* (2014) Enhanced sulfate formation during China's severe winter haze episode in January 2013 missing from current models. *J. Geophys. Res. Atmos.* 119(17):10,425-410,440.
37. Zheng B*, et al.* (2015) Heterogeneous chemistry: a mechanism missing in current models to explain secondary inorganic aerosol formation during the January 2013 haze episode in North China. *Atmos. Chem. Phys.* 15(4):2031-2049.
38. Wang Z, Akimoto H, & Uno I (2002) Neutralization of soil aerosol and its impact on the distribution of acid rain over east Asia: Observations and model results. *J. Geophys. Res. Atmos.* 107(D19):ACH 6-1-ACH 6-12.
39. Zhang XY*, et al.* (2012) Atmospheric aerosol compositions in China: spatial/temporal variability, chemical signature, regional haze distribution and comparisons with global aerosols. *Atmos. Chem. Phys.* 12(2):779-799.
40. Wen W, Cheng S, Liu L, Wang G, & Wang X (2016) Source apportionment of PM2.5 in Tangshan, China—Hybrid approaches for primary and secondary species apportionment. *Front. Environ. Sci. Eng.* 10(5):6.
41. Cao JJ*, et al.* (2005) Characterization and source apportionment of atmospheric organic and elemental carbon during fall and winter of 2003 in Xi'an, China. *Atmos. Chem. Phys.* 5(11):3127-3137.
42. Ding A*, et al.* (2016) Long-term observation of air pollution-weather/climate interactions at the SORPES station: a review and outlook. *Front. Environ. Sci. Eng.* 10(5):15.
43. Wang Q*, et al.* (2019) Source apportionment of fine particulate matter in Macao, China with and without organic tracers: A comparative study using positive matrix factorization. *Atmos. Environ.* 198:183-193.
44. Wang H*, et al.* (2018) Seasonal characteristics, formation mechanisms and source origins of PM2.5 in two megacities in Sichuan Basin, China. *Atmos. Chem. Phys.* 18(2):865-881.
45. Huang X-F*, et al.* (2018) Exploration of PM2.5 sources on the regional scale in the Pearl River Delta based on ME-2 modeling. *Atmos. Chem. Phys.* 18(16):11563-11580.
46. Tang J, Xu X, Ba J, & Wang S (2010) Trends of the precipitation acidity over

China during 1992–2006. *Chin. Sci. Bull.* 55(17):1800-1807.
47. Pan Y*, et al.* (2018) Identifying Ammonia Hotspots in China Using a National Observation Network. *Environ. Sci. Technol.* 52(7):3926-3934.
48. Van Damme M*, et al.* (2015) Towards validation of ammonia (NH3) measurements from the IASI satellite. *Atmos. Meas. Tech.* 8(3):1575-1591.
49. Clarisse L, Clerbaux C, Dentener F, Hurtmans D, & Coheur P-F (2009) Global ammonia distribution derived from infrared satellite observations. *Nat. Geosci.* 2(7):479-483.
50. Van Damme M*, et al.* (2017) Version 2 of the IASI NH3 neural network retrieval algorithm: near-real-time and reanalysed datasets. *Atmos. Meas. Tech.* 10(12):4905-4914.
51. Liu M*, et al.* (2017) Fine particle pH during severe haze episodes in northern China. *Geophys. Res. Lett.* 44(10):5213-5221.
52. Hung HM, Hsu MN, & Hoffmann MR (2018) Quantification of SO2 Oxidation on Interfacial Surfaces of Acidic Micro-Droplets: Implication for Ambient Sulfate Formation. *Environ. Sci. Technol.* 52(16):9079-9086.
53. Steeneveld G-J (2014) Current challenges in understanding and forecasting stable boundary layers over land and ice. *Front. Environ. Sci.* 2(41).
54. Wang H*, et al.* (2015) Mesoscale modelling study of the interactions between aerosols and PBL meteorology during a haze episode in China Jing–Jin–Ji and its near surrounding region – Part 2: Aerosols' radiative feedback effects. *Atmos. Chem. Phys.* 15(6):3277-3287.
55. Wang H*, et al.* (2018) Contributions to the explosive growth of PM2.5 mass due to aerosol–radiation feedback and decrease in turbulent diffusion during a red alert heavy haze in Beijing–Tianjin–Hebei, China. *Atmos. Chem. Phys.* 18(23):17717-17733.
56. Klimont Z & Winiwarter W (2011) Integrated Ammonia Abatement - Modelling of Emission Control Potentials and Costs in GAINS, IIASA Interim Report. (International Institute for Applied Systems Analysis (IIASA), Laxenburg, Austria).
57. Liu J, Han Y, Tang X, Zhu J, & Zhu T (2016) Estimating adult mortality attributable to PM2.5 exposure in China with assimilated PM2.5 concentrations based on a ground monitoring network. *Sci. Total Environ.* 568:1253-1262.
58. Lelieveld J, Evans JS, Fnais M, Giannadaki D, & Pozzer A (2015) The contribution of outdoor air pollution sources to premature mortality on a global scale. *Nature* 525(7569):367-371.
59. Evans J*, et al.* (2013) Estimates of global mortality attributable to particulate air pollution using satellite imagery. *Environ. Res.* 120:33-42.
60. Anenberg SC, Horowitz LW, Tong DQ, & West JJ (2010) An estimate of the global burden of anthropogenic ozone and fine particulate matter on premature human mortality using atmospheric modeling. *Environ. Health Perspect.*

118(9):1189.
61. Elfadel M & Massoud M (2000) Particulate matter in urban areas: health-based economic assessment. *Sci. Total Environ.* 257(2-3):133.
62. López MT*, et al.* (2005) Health impacts from power plant emissions in Mexico. *Atmos. Environ.* 39(7):1199-1209.
63. Kan H & Chen B (2004) Particulate air pollution in urban areas of Shanghai, China: health-based economic assessment. *Sci. Total Environ.* 322(1-3):71.
64. Wang H & Mullahy J (2006) Willingness to pay for reducing fatal risk by improving air quality: a contingent valuation study in Chongqing, China. *Sci. Total Environ.* 367(1):50.
65. Zhang M, Song Y, & Cai X (2007) A health-based assessment of particulate air pollution in urban areas of Beijing in 2000-2004. *Sci. Total Environ.* 376(1–3):100-108.
66. Xu X, Chen R, Kan H, & Ying X (2013) Meta-analysis of contingent valuation studies on air pollution-related value of statistical life in China (in Chinese). *Chinese Health Resources*.
67. Singh A & Agrawal M (1996) Response of two cultivars of Triticum aestivum L. to simulated acid rain. *Environ. Pollut.* 91(2):161-167.
68. Evans LS, Lewin KF, Owen EM, & Santucci KA (1986) Comparison of Yields of Several Cultivars of Field-Grown Soybeans Exposed to Simulated Acidic Rainfalls. *New Phytol.* 102(3):409-417.
69. Feng Z, Miao H, Zhang F, & Huang Y (2002) Effects of acid deposition on terrestrial ecosystems and their rehabilitation strategies in China. *J. Environ. Sci.* 14(2):227-233.
70. Lei L & Yuan H (2016) *China Agriculture Yearbook for 2015 (in Chinese)* (China Agriculture Press, Beijing, China).
71. Mahapatra AK & Tewari DD (2005) Importance of non-timber forest products in the economic valuation of dry deciduous forests of India. *Forest Policy and Economics* 7(3):455-467.
72. Sutton MA*, et al.* (2011) *The European Nitrogen Assessment: Costs and benefi ts of nitrogen in the environment* (Cambridge University Press) pp 513-540.
73. Posch M, Duan L, Reinds GJ, & Zhao Y (2015) Critical loads of nitrogen and sulphur to avert acidification and eutrophication in Europe and China. *Landscape Ecology* 30(3):487-499.
74. Klimont Z & Brink C (2004) Modelling of Emissions of Air Pollutants and Greenhouse Gases From Agricultural Sources in Europe. *Environmental Effects on Spacecraft Positioning & Trajectories*:131-137.
75. Sommer SG & Hutchings NJ (2001) Ammonia emission from field applied manure and its reduction—invited paper. *Eur. J. Agron.* 15(1):1-15.
76. Bouwman AF*, et al.* (1997) A global high-resolution emission inventory for ammonia. *Global Biogeochem. Cy.* 11(4):561-587.
77. van Grinsven HJM*, et al.* (2015) Losses of Ammonia and Nitrate from

Agriculture and Their Effect on Nitrogen Recovery in the European Union and the United States between 1900 and 2050. *J. Environ. Qual.* 44(2):356-367.